5014–5028 *Nucleic Acids Research, 2022, Vol. 50, No. 9* *Published online 30 April 2022*
https://doi.org/10.1093/nar/gkac293

Phosphorylation of the FACT histone chaperone subunit SPT16 affects chromatin at RNA polymerase II transcriptional start sites in *Arabidopsis*

Philipp Michl-Holzinger[1], Simon Obermeyer[1], Hanna Markusch[1], Alexander Pfab[1], Andreas Ettner[1], Astrid Bruckmann[2], Sabrina Babl[3], Gernot Längst[3], Uwe Schwartz[4], Andrey Tvardovskiy[5], Ole N. Jensen[5], Akihisa Osakabe[6], Frédéric Berger[6] and Klaus D. Grasser[1,*]

[1]Department of Cell Biology & Plant Biochemistry, Centre for Biochemistry, University of Regensburg, Universitätsstr. 31, D-93053 Regensburg, Germany, [2]Institute for Biochemistry I, Centre for Biochemistry, University of Regensburg, Universitätsstr. 31, D-93053 Regensburg, Germany, [3]Institute for Biochemistry III, Centre for Biochemistry, University of Regensburg, Universitätsstr. 31, D-93053 Regensburg, Germany, [4]NGS Analysis Centre, Biology and Pre-Clinical Medicine, University of Regensburg, Universitätsstr. 31, D-93053 Regensburg, Germany, [5]Department of Biochemistry and Molecular Biology, VILLUM Center for Bioanalytical Sciences, University of Southern Denmark, Odense, Denmark and [6]Gregor Mendel Institute (GMI), Austrian Academy of Sciences, Vienna BioCenter (VBC), Dr. Bohr-Gasse 3, 1030 Vienna, Austria

Received September 15, 2021; Revised April 12, 2022; Editorial Decision April 13, 2022; Accepted April 19, 2022

ABSTRACT

The heterodimeric histone chaperone FACT, consisting of SSRP1 and SPT16, contributes to dynamic nucleosome rearrangements during various DNA-dependent processes including transcription. In search of post-translational modifications that may regulate the activity of FACT, SSRP1 and SPT16 were isolated from *Arabidopsis* cells and analysed by mass spectrometry. Four acetylated lysine residues could be mapped within the basic C-terminal region of SSRP1, while three phosphorylated serine/threonine residues were identified in the acidic C-terminal region of SPT16. Mutational analysis of the SSRP1 acetylation sites revealed only mild effects. However, phosphorylation of SPT16 that is catalysed by protein kinase CK2, modulates histone interactions. A non-phosphorylatable version of SPT16 displayed reduced histone binding and proved inactive in complementing the growth and developmental phenotypes of *spt16* mutant plants. In plants expressing the non-phosphorylatable SPT16 version we detected at a subset of genes enrichment of histone H3 directly upstream of RNA polymerase II transcriptional start sites (TSSs) in a region that usually is nucleosome-depleted. This suggests that some genes require phosphorylation of the SPT16 acidic region for establishing the correct nucleosome occupancy at the TSS of active genes.

INTRODUCTION

Packaging nuclear DNA into nucleosomes constitutes the basic structural unit of eukaryotic chromatin. Due to their stability, nucleosomes serve as general repressors of transcription and other DNA-dependent processes (1,2). Accordingly, various mechanisms exist that facilitate the transcription of chromatin templates by destabilization/disassembly of nucleosomes (3). So-called histone chaperones play a fundamental role in regulating nucleosomal dynamics. They represent a diverse group of proteins that functionally interact with core histones to assemble/disassemble nucleosome particles without consuming energy in form of ATP. In this way, histone chaperones are key factors that determine nucleosome properties, for instance, by modulating the distribution of histone variants or epigenetic information, thereby defining functionally distinct chromatin landscapes (4–6).

FACT is a heterodimeric histone chaperone consisting of SSRP1 (Pob3 in yeast) and SPT16 that originally was identified in yeast and mammalian cells (7–10). Its established name traces back to the finding that FACT facilitates chromatin transcription by promoting *in vitro* transcription by RNA polymerase II (RNAPII) from reconstituted chromatin templates. Meanwhile it became apparent that

*To whom correspondence should be addressed. Tel: +49 941 9433032; Fax: +49 941 9433353; Email: klaus.grasser@biologie.uni-regensburg.de
Present address: Andrey Tvardovskiy, Institute of Functional Epigenetics, Helmholtz Zentrum München, 85764 Neuherberg, Germany.

FACT contributes to other chromatin-dependent processes including recombination, replication and repair (11–14), and hence the established abbreviation may well stand more broadly for facilitates chromatin transactions. Regarding transcription by RNAPII, FACT has been implicated in initiation (15–18) as well as in the elongation stage (8,9,19,20). Importantly, FACT can disassemble and reassemble nucleosomes; thereby it is involved in both overcoming and maintaining the nucleosomal barrier to DNA-dependent processes in the chromatin context. To accomplish that, FACT establishes contacts with different nucleosomal targets including H2A–H2B dimers, H3–H4 tetramers and DNA (21–26). A recent structural analysis of FACT in complex with nucleosomal particles revealed that the overall shape of FACT resembles a unicycle, consisting of a saddle and fork that is engaged in multiple interactions with histones and DNA (27). Reversible nucleosome reorganization and uncoiling of nucleosomal DNA from the histone core, increasing DNA accessibility, are brought about by FACT interfering with DNA-histone contacts (24,25,28,29). Moreover, FACT plays a critical role in nucleosome reassembly, for instance, following RNAPII passage to maintain chromatin signature and to repress transcription initiation from cryptic sites within coding regions (25,30–32).

In plants, there is also a variety of histone chaperones (33,34) and their loss affects regulation of growth and development or the response to environmental stress conditions (35–37). Likewise, FACT consisting of SSRP1 and SPT16 is conserved in a wide variety of plant species (38,39). Both subunits are essential for viability in *Arabidopsis* (40,41) and are widely expressed in almost all cell types (42–44). Plants deficient in SSRP1 or SPT16 display various defects in vegetative and reproductive development including increased number of leaves and inflorescences, early flowering, reduced seed production and impairment of proper expression of parentally regulated genes during seed development (40,41,43). FACT copurified with the RNAPII transcript elongation complex from *Arabidopsis* cells and associated with active protein-coding genes in a transcription dependent manner (41,42,45–47), suggesting a role in transcriptional elongation. At the same time *Arabidopsis* FACT efficiently represses intragenic transcriptional initiation (48).

Currently, there is only limited information about the potential regulation of FACT function via post-translational modifications (12). Protein kinase CK2 *in vitro* phosphorylates human and maize SSRP1 altering DNA interactions of the protein (49,50). *Drosophila* SSRP1 is phosphorylated at CK2 consensus sites in insect cells and the phosphorylation has subtle effects on *in vitro* nucleosome interactions of SSRP1 (51,52). Human SPT16 is phosphorylated within its acidic domain in insect cells and the phosphorylation influences the interaction with a 112-bp octasome (23). Since plant FACT has not been systematically analysed for post-translational modifications and their function, we isolated both subunits from *Arabidopsis* cells and using mass spectrometry four acetylation sites were detected in SSRP1, while three phosphorylation sites were mapped in SPT16. Mutation of the SSRP1 acetylation sites revealed only mild effects, whereas mutation of the SPT16 phosphorylation sites affected its interaction with histones and the ability of the protein to complement efficiently the mutant phenotype of *spt16* plants. In addition, the expression of a non-phosphorylatable SPT16 variant resulted in a distinct histone H3 enrichment upstream of RNAPII transcriptional start sites (TSSs) of a subset of genes.

MATERIALS AND METHODS

Plasmid constructions

The required gene or cDNA sequences were amplified by PCR with KAPA DNA polymerase (PeqLab) using an *Arabidopsis thaliana* genomic DNA or cDNA as template and the primers (providing also the required restriction enzyme cleavage sites) listed in Supplementary Table S1. Mutations were introduced by overlap extension PCR. The PCR fragments were inserted into suitable plasmids using standard methods. All plasmid constructions were checked by DNA sequencing, and details of the plasmids generated in this work are summarized in Supplementary Table S2.

Plant material

Seeds of *Arabidopsis thaliana* (Col-0, L*er*) were stratified in darkness for 48 h at 4°C and plants were grown at 21°C on soil in a phytochamber or on MS medium in plant incubators under long-day conditions (45,53). The T-DNA insertion lines *ssrp1-1* and *spt16-1* used for the presented experiments were previously reported (41). *Agrobacterium*-mediated plant transformation, characterization of transgenic lines and PCR-based genotyping of plants using primers specific for DNA insertions and target genes (Supplementary Table S1) was performed as previously described (53,54). Primary transformants were selected and analysed by PCR-based genotyping. Plants harbouring the transgene were screened by immunoblotting for uniform expression and were examined for consistent phenotype. Based on these analyses three independent plant lines per transgene were typically selected for further experimentation, of which one line was analysed in detail. Plant phenotypes were observed and documented as previously described (41,53), while some analyses were performed using the software Leaf-GP (55).

Affinity purification and characterization of GS-tagged proteins from *Arabidopsis* cells

Arabidopsis suspension cultured PSB-D cells were maintained and transformed as previously described (56). Proteins of 15 g cultured cells were isolated and GS-tagged proteins (2× protein G domains and streptavidin-binding peptide) were purified by IgG affinity chromatography as previously described (45,53). 1.5 μg of in solution trypsin digested sample were analysed by LC–MS/MS using a Proxeon Easy nLC system (Thermo Scientific) essentially as previously described (57). Samples were loaded through a two-column system (analytical- (15 cm) and trap-column (3 cm) with an internal diameter of 75 μm filled C18-AQ 3 μm (150 × 4 mm) ReproSil-Pur beads. Separations were performed using gradient elution at RT with a flow rate of 300 nl/min. The mobile phase consisted of a linear gradient containing 0.1% formic acid (v/v) (eluent A) and 0.1%

formic acid in 95% acetonitrile (eluent B). The LC system was coupled to a Q Exactive hybrid quadrupole-Orbitrap mass spectrometer (Thermo Scientific) via an electrospray ionization source operated in positive ion mode. Mass spectra were acquired using a top 12 high collision dissociation (HCD) data-dependent acquisition (DDA) method. The obtained peptide mass fingerprints were analysed using the proteome discoverer 2.0 software, searching the UniProt database. Enzyme specificity was set to trypsin allowing up to two missed cleavages. The search included cysteine carbamidomethylation as a fixed modification, protein N-terminal acetylation, acetylation of lysine and arginine, mono-, di- and tri- methylation of lysine, mono- and dimethylation of arginine, oxidation of methionine and phosphorylation of serine, threonine, and tyrosine as variable modifications. Peptide identification was based on a search with a mass deviation of the precursor ion up to 2.5 ppm after recalibration, and the allowed fragment mass deviation was set to 0.01 Da. Analysis of *in vitro* phosphorylated proteins and subtraction of the experimental background of contaminating proteins were performed as previously described (45).

Antibodies and immunoblotting

For immunoblotting, the following primary and secondary antibodies were used: anti-H2B (cat. no. ab1790, Abcam) and anti-H3 (cat. no. ab1791, Abcam); anti-SSRP1 and anti-SPT16 (42); secondary HRP-coupled α-rabbit antibody (Sigma Aldrich). Total protein extracts from PSB-D cultures were prepared as described before (45) and nuclear proteins were isolated as for ChIP (53,58). Following SDS-PAGE proteins were electro-transferred onto a PVDF membrane. For immunoblot analysis SuperSignal R West Pico Chemiluminescent substrate (Thermo Fisher Scientific) was used and chemiluminescence was detected using a Multiimage FluorChem FC2 instrument (Alpha Innotech) or the ChemiDoc MP system (Bio-Rad).

Recombinant proteins

Using the respective expression vectors (Supplementary Table S2) truncated/mutated SSRP1 proteins were expressed in *E. coli* as 6xHis-tagged fusion proteins that were purified by two-step chromatography (Ni-NTA–agarose, phenyl-sepharose) as previously described (59). Using the respective expression vectors (Supplementary Table S2) truncated/mutated SPT16 proteins were expressed in *Escherichia coli* as 6xHis-tagged or glutathione S transferase (GST) tagged fusion proteins that were purified by Ni-NTA–agarose or glutathione-sepharose chromatographies, respectively, as previously described (53,59). Recombinant *Arabidopsis* and human histones H2A–H2B were prepared as previously described (60,61), while recombinant maize CK2α was purified by three-step chromatography as previously described (62).

Circular dichroism (CD)

Proteins (10 μM) were analysed in 50 mM KH_2PO_4 using a Jasco J-815 CD spectropolarimeter using a 0.02 cm cell. The buffer signal was subtracted and the measured ellipticity was converted into mean residue ellipticity as described before (63).

Electrophoretic mobility shift assay (EMSA)

DNA and different concentrations of protein were incubated in 1x EMSA buffer (10 mM Tris–HCl pH 7.5, 50 mM NaCl, 5 mM $MgCl_2$, 1 mM EDTA, 1 mM DTT, 5% (v/v) glycerol, 0.01 mg/ml BSA) for 10 min and analysed in 6% polyacrylamide TBE gels. DNA was visualized using ethidium bromide staining.

GST pull-down assays

Recombinant SPT16 proteins fused to glutathione S transferase (GST) were mixed with equimolar amounts of recombinant *Arabidopsis* H2A–H2B or with bovine cytochrome *c* (Sigma Aldrich) in GST buffer (0.2–0.35 M NaCl, 25 mM HEPES pH 7.6, 0.05% (v/v) NP40, 5 mM DTT, 10% (v/v) glycerol, 2 mM $MgCl_2$). For some assays GST-AD/WT was phosphorylated *in vitro* by CK2α (as described below) prior to the binding reaction. Following incubation (30 min at 30°C) glutathione sepharose beads were added and the samples were incubated for 3 h on a rotating wheel at 4°C. Beads were washed three times in GST buffer before bound proteins were eluted by boiling in protein loading buffer and analysed by SDS-PAGE.

MicroScale thermophoresis (MST)

For MST, GST-AD proteins were labelled with a 647-NHS-ester (Dyomics). MST experiments were performed in MST buffer (200 mM NaCl, 2.7 mM KCl, 10 mM Na_2HPO_4, 1.8 mM KH_2PO_4, pH 7.4) with constant target concentration of 10 nM and a 1:2 ligand titration starting at 36 μM H2A–H2B. Measurements were performed in premium capillaries at 7% LED, 60% MST at 25°C on a Monolith NT.115_{Pico} device (NanoTemper Technologies). The data was analyzed using the MO.affinity analysis software (NanoTemper Technologies) and binding affinity was determined at 2.5s laser On time. Data was fitted using the K_D model and fraction bound was calculated by dividing the ΔF_{norm} value of each point by the amplitude of the fitted curve, resulting in values from 0 to 1 (0 = unbound, 1 = bound).

Protein kinase CK2 *in vitro* phosphorylation assays

Radioactive and non-radioactive CK2 phosphorylation assays were performed as previously described (62). For radioactive assays, recombinant SPT16 proteins were reacted in the presence of [γ-^{32}P]ATP with recombinant maize CK2α. Phosphate incorporation was monitored by SDS-PAGE and scanning of the gels using a Cyclone Storage phosphorimager (Canberra Packard). For non-radioactive assays, recombinant SPT16 proteins were phosphorylated by recombinant purified maize CK2α in the presence of unlabelled ATP and phosphate incorporation was monitored by acetic acid urea PAGE (AU-PAGE) (64) and by mass spectrometry.

Chromatin immunoprecipitation (ChIP)

ChIP was essentially performed as previously described (53,58) using 1 g of 14-days after stratification (14-DAS) *in vitro* grown plants that were crosslinked with 1% (v/v) formaldehyde. Chromatin was sonicated using a Bioruptor Pico (Diagenode) and immunoprecipitation with antibodies specific for the C-terminal part of histone H3 (cat. no. ab1791, Abcam) was performed using magnetic Dynabeads Protein A (Thermo Fisher Scientific). To generate libraries for high-throughput sequencing the NEBNext Ultra II DNA Library Prep Kit with index primers NEBNext multiplex oligos for Illumina (New England BioLabs) were used. Sequencing of the libraries (75-nt, single-end) was performed by the Genomics Core Facility at the University of Regensburg (http://www.kfb-regensburg.de/) using an Illumina NextSeq 500 instrument. Reads were aligned to the TAIR10 genome (https://www.arabidopsis.org/) using Bowtie2 (65) and coverage tracks were calculated with DANPOS2 (66). Downstream analysis was mainly performed using the deepTools2 suite (version 3.5.0) (67) and quality control was performed at several steps using FastQC (68). Three replicates were obtained for each genotype and 12.6–16.2 million reads per sample mapped uniquely to the *Arabidopsis* genome (average Phred quality score >34 for each library). Expression levels of genes (divided into quartiles according to logTPM) was deduced from RNA sequencing data of *in vitro* grown 6-DAS Col plants (NCBI sequence read archive, PRJNA758800). MNase sequencing data (69) were reanalysed. After preprocessing reads were aligned to the *Arabidopsis* TAIR10 genome using Bowtie2 (65). Only reads with mononucleosomal length (140–200 bp) were used for further analysis and genome-wide nucleosome occupancy maps were generated using the dpos option of the DANPOS2 (66).

RESULTS

Mapping post-translational modifications of the FACT subunits

To identify post-translational modifications of the FACT subunits, SSRP1 and SPT16 were isolated from *Arabidopsis* suspension cultured cells. We used PSB-D cell lines expressing SSRP1 or SPT16 fused to a GS affinity tag as well as cells expressing the unfused GS tag that served as a control (45). GS fusion proteins (and the unfused GS tag) were isolated from total protein extracts by IgG affinity purification (45,53) and analysed by SDS-PAGE. Several prominent protein bands co-eluted with SSRP1-GS and SPT16-GS (Figure 1A). Notably, SSRP1 and SPT16 co-purified with each other, as expected (42), and histones were found to be enriched in the eluates. Subsequently, the eluted proteins were digested with trypsin and analysed by liquid chromatography coupled with mass spectrometry (LC–MS). Modified peptides detected with high confidence (FDR < 0.01) were considered. The mass spectrometric analyses revealed four acetylation sites mapping to lysine residues (Supplementary Figure S1A) in the HMG-box domain of SSRP1 (K594, K599) and to the flanking basic region (K539, K549) (Figure 1B, C). SSRP1 proteins of various plant species contain lysine residues at respective positions. Moreover, two high-confidence phosphorylation sites map to serine residues (Supplementary Figure S1B) within the intrinsically disordered acidic domain of SPT16 (S1033, S1035) (Figure 1B,C). An additional phosphorylation site (T1023) adjacent to the phospho-serine was detected with lower confidence, but it is indicated in our data, since it was also identified in our *in vitro* phosphorylation experiments (see below).

Mild effects caused by acetylation of SSRP1

Since protein acetylation can alter functional properties of diverse HMG-box proteins including their DNA interactions (70,71), we produced different recombinant SSRP1 proteins comprising the C-terminal region including the HMG-box DNA-binding domain (DBD). In addition to the wild-type variant (DBD/WT), we generated proteins in which the four acetylated lysines (Supplementary Figure S2A, B) were changed to non-acetylatable alanine or to acetylation-mimicking glutamine residues (DBD/4xA or DBD/4xQ, respectively). Proteins purified by two-step chromatography (Supplementary Figure S2C) were analysed for possible structural differences using CD spectroscopy and for their DNA-binding capacities using electrophoretic mobility shift assays (EMSAs). Far-UV CD spectra of the three proteins (Supplementary Figure S2D) reflect the largely α-helical structure of HMG-box domains (72,73). Relative to DBD/WT the spectra of the mutated proteins indicate some loss in the amount of α-helix (mild decrease of the negative peak around 222 nm) and a gain in random coil (minimum around 200 nm). HMG-box proteins often bind selectively to certain DNA structures including DNA minicircles or four-way junction (4wj) DNA (72,73). Therefore, we reacted increasing concentrations of the recombinant proteins with 4wj DNA. As evident from the disappearance of the unbound DNA probe and the formation of protein complexes with lower electrophoretic mobility, the three variants displayed no clear differences in their affinity for the 4wj DNA (Supplementary Figure S2E). Relative to the WT protein, we observed with the mutant variants a reduced tendency of forming distinctly recognisable protein/DNA complexes in the EMSA analysis. Similarly, the affinity of the mutant variants for linear DNA differed only slightly from that of the WT protein (Supplementary Figure S2F).

Acetylation of HMG-box proteins can influence their subcellular localization, as exemplified by mammalian HMGB1 (74). Moreover, two of the identified SSRP1 acetylation sites are situated within a 20-aa basic region adjacent to the HMG-box domain (cf. Supplementary Figure S2A), which serves as nuclear localization sequence in maize SSRP1 (75). Therefore, SSRP1/WT and the mutant version SSRP1/4xQ both fused to eGFP were expressed in Col-0 plants. Analysis of leaf cells of the transgenic plants by confocal laser scanning microscopy (CLSM) demonstrated that both eGFP fusion proteins localize to the nucleus (Supplementary Figure S3A), suggesting that the acetylatable lysine residues do not interfere with nuclear localization.

To explore the potential role of the identified acetylatable residues of SSRP1 in plant growth and development, we used a complementation approach. The *Arabidopsis* trans-

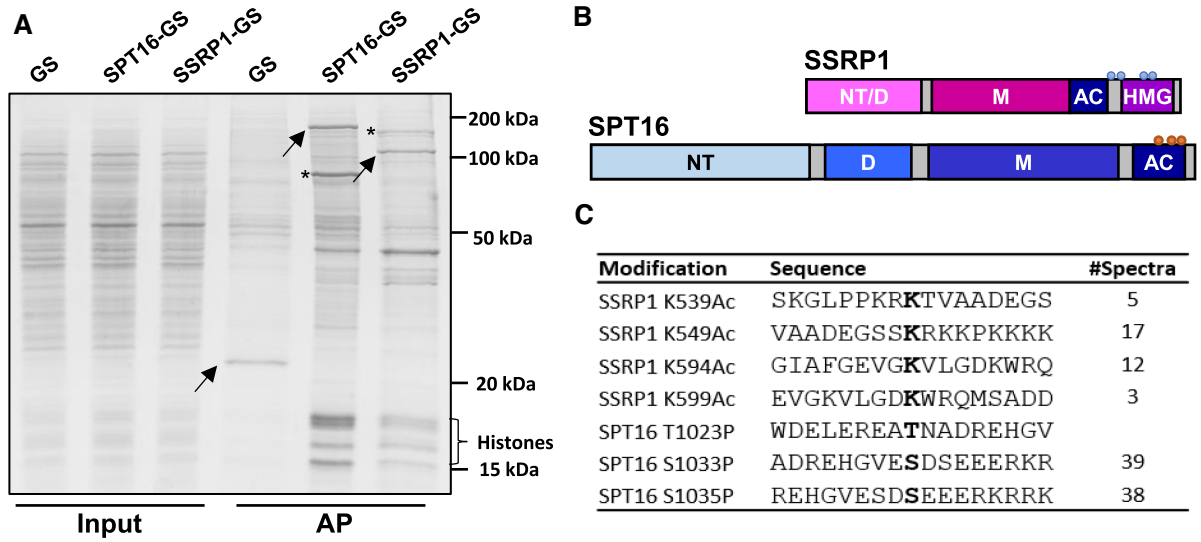

Figure 1. Mapping of acetylation sites in SSRP1 and phosphorylation sites in SPT16. (**A**) Affinity purification of FACT subunits from Arabidopsis cells. The indicated GS-fusion proteins were purified from PSB-D cells by IgG affinity chromatography from total protein extracts. Isolated proteins were separated by SDS-PAGE and stained with Coomassie brilliant blue. The unfused GS-tag (GS) served as control in these experiments. Arrows indicate the bands corresponding to the bait proteins fused to the GS-tag. Asterisks indicate the respective complex partner. (**B**) Schematic representation of the SSRP1 and SPT16. SSRP1 is composed of an N-terminal domain (that is required for heterodimerization (NT/D) with SPT16), middle domain (M), acidic region (AC) and HMG-box domain (HMG), while SPT16 consists of N-terminal (NT), dimerization (D), middle (M), and acidic (AC) domains. (**C**) MS analysis lead to the detection of acetylation and phosphorylation sites in SSRP1 and SPT16, respectively. The list summarizes the modified sites (bold) that were identified in the MS analyses. Shown are modifications, which were found in more than one high confidence spectrum, except T1023P which was detected with low confidence and included here because of additional results (see below). The identified modified residues are indicated in the scheme in (B) with acetylation sites in SSRP1 (lysine, blue circles) and phosphorylation sites in SPT16 (serine/threonine, orange circles).

poson insertion mutant *ssrp1-1* is homozygous lethal and exhibits wild-type phenotype in the heterozygous state (41). Constructs driving the expression of wild-type SSRP1/WT or of the mutated SSRP1/4xR and SSRP1/4xQ variants were introduced into heterozygous *ssrp1-1* plants. The presence of the three complementation constructs allowed the isolation of plants homozygous for the *ssrp1-1* mutation (Supplementary Figure S3B), demonstrating that the expression of SSRP1 and the mutant variants restored growth of the otherwise lethal *ssrp1-1* mutant. The SSRP1 proteins were expressed at similar levels in the different plant lines (Supplementary Figure S3C). Comparative phenotypic analysis of the L*er* wild-type control along with the complementation lines illustrated that all plants basically had wild-type appearance (Figure 2A). No striking differences were observed between the plant lines regarding bolting time of the plants or various growth determinants including leaf area and height of the plants (Figure 2B)—parameters that are clearly affected with homozygous viable plants of the *ssrp1-2* allele (41). We concluded that although acetylation of SSRP1 affects to some extent protein structure and its interaction with DNA, our analyses did not reveal distinct impact of the identified acetylatable residues in SSRP1 on plant growth and development under standard growth conditions.

SPT16 is phosphorylated by protein kinase CK2

Inspection of the amino acid sequence around the serine residues in SPT16 identified as phospho-sites, revealed that S1033/S1035 are situated within consensus phosphorylation sites of protein kinase CK2 (Figure 3A). Target sites of CK2 often reside in acidic regions of substrate proteins within a minimal consensus sequence (i.e. S/T-X-X-D/E/pS) (76). To examine the *in vitro* capacity of CK2 to phosphorylate SPT16, the acidic domain (AD, D955-R1075) was generated as 6xHis-tagged protein. The purified protein was incubated with the recombinant catalytic subunit (CK2α) of maize CK2 in the presence of radiolabelled ATP. Separation of the phosphorylation reactions by SDS-PAGE and visualization of the ^{32}P-incorporation into the substrate protein demonstrated that CK2α efficiently phosphorylated the acidic domain of SPT16 (Figure 3B). Phosphorylation of the acidic domain by CK2α in the presence of unlabelled ATP did not alter the electrophoretic mobility of the protein compared to the non-phosphorylated protein in SDS-PAGE analysis, whereas phosphorylation by CK2α resulted in a clear mobility shift of SPT16-AD in acetic acid urea PAGE analysis (Figure 3C). To identify sites phosphorylated by CK2α *in vitro*, the phosphorylated acidic domain (as in Figure 3C) was proteolytically cleaved and analysed by LC–MS. Mass spectrometric analyses demonstrated that in addition to serine residues S1033/S1035, threonine T1023 was distinctly phosphorylated in our *in vitro* phosphorylation assay (Figure 3D). Since the same phospho-sites were detected on SPT16 isolated from *Arabidopsis* cells, it was likely that protein kinase CK2 phosphorylates SPT16 *in planta*. In support of this idea, several CK2 variants robustly co-purified with SPT16-GS and SSRP1-GS in our AP-MS analyses of *Arabidopsis* cells (Supplementary Table S3). Since the acidic domain of SPT16 contains several additional CK2 consensus sites (Figure 3A), we wondered whether (some of) these sites may be also phosphorylated by CK2, but perhaps escape

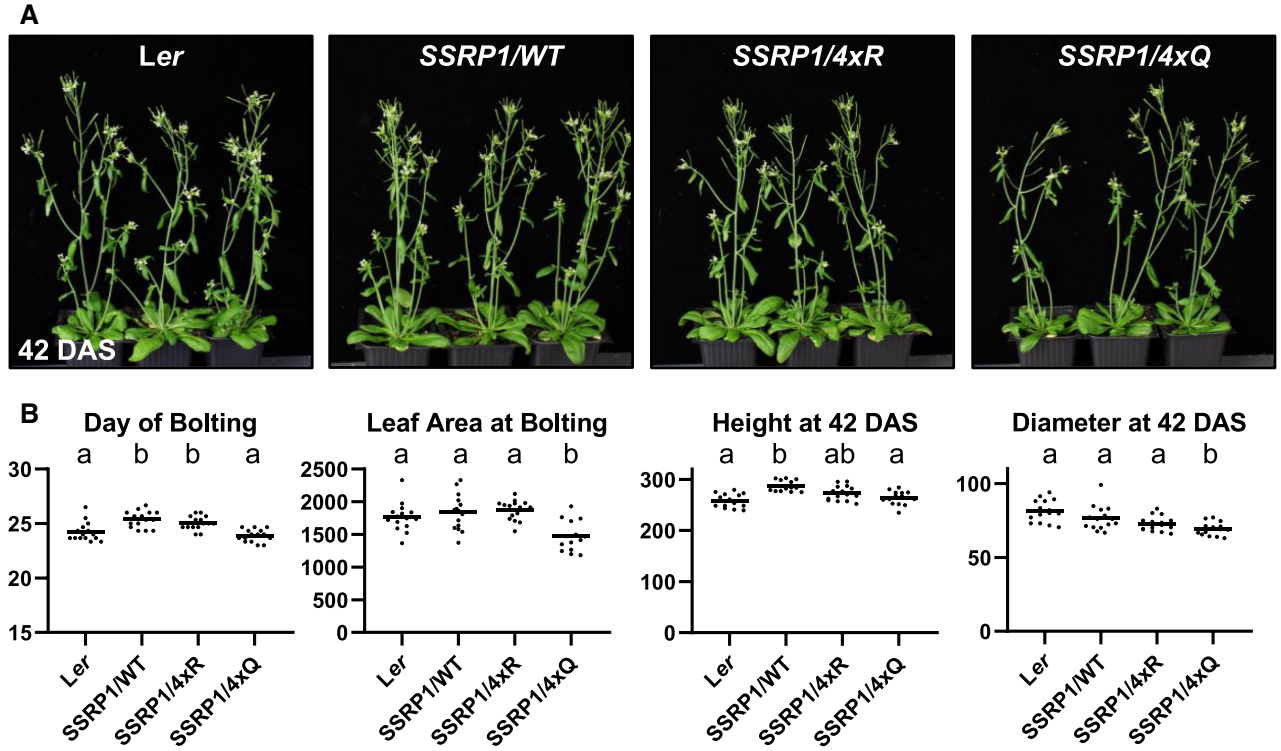

Figure 2. Plants expressing SSRP1 acetylation site mutants are mildly affected. Plants of the *ssrp1-1* mutant line were transformed with constructs driving the expression of wild-type SSRP1 (SSRP1/WT), the four acetylated lysine residues changed to arginine (K539R/K549R/K594R/K599R, termed SSRP1/4xR) or the four acetylated lysine residues changed to glutamine (K539Q/K549Q/K594Q/K599Q, termed SSRP1/4xQ) and were phenotypically analysed relative to the wild-type (L*er*). (**A**) Representative individuals of the different transgenic lines relative to L*er* (42 DAS) are shown. (**B**) Quantification of phenotypic parameters. Day of bolting, leaf area at bolting [mm2], height at 42 DAS [mm], rosette diameter at 42 DAS [mm], were determined. Data comprised the measurements of 15 individual plants of each genotype in three biological replicates and was analysed by one-way ANOVA. The line in the scatterplot marks the average value and letters above the scatter indicate the outcome of the Tukey´s test (P-value < 0.05).

mass spectrometric detection. Therefore, a mutated version of the acidic domain (with non-phosphorylatable changes in T1023V, S1033A, S1035A termed AD/VAA) was generated (Supplementary Figure S4A). The mutated version and the wild-type acidic domain were comparatively phosphorylated using the *in vitro* ^{32}P-CK2α assay (Supplementary Figure S4B). Relative to the wild-type protein the mutated version was phosphorylated to a lesser extent. Quantification of the ^{32}P-incorporation demonstrated that phosphorylation is decreased by ∼40% (Supplementary Figure S4C). This illustrates that the three identified residues are target sites of CK2, but additional residues within the acidic domain can be phosphorylated by this protein kinase, although the corresponding phospho-peptides were not detected in our LC–MS analyses of SPT16 isolated from plant cells. This could be related to low stoichiometry of the *in vivo* phosphorylations, or technical issues including ion suppression and the fact that the peptides are highly negatively charged.

Influence of phosphorylation on SPT16 interaction with histones

The acidic domain of SPT16 substantially contributes to FACT-histone interactions (22,24,26). To examine whether the phosphorylation of the acidic domain alters histone binding, we produced a non-phosphorylatable and a phosphomimic variant of the acidic domain (AD) by replacing the phosphorylated S/T residues as above (T1023V, S1033A, S1035A termed AD/VAA) or with acidic residues (T1023E, S1033D, S1035D, termed AD/EDD), respectively. Recombinant AD/VAA, AD/EDD and wild-type versions of the acidic domain fused to GST were expressed in *E. coli* and purified. The three GST-AD fusion proteins along with unfused GST and potential binding partners, heterodimers of recombinant *Arabidopsis* histone H2A and H2B and cytochrome C (CytC) were analysed by SDS-PAGE (Figure 4A), illustrating their purity. The GST-AD proteins were used for GST pull-down assays with histone H2A–H2B. Histones were incubated with GST-AD/WT, GST-AD/VAA and GST-AD/EDD at different NaCl concentrations. Following immobilization on glutathione sepharose beads and washing of the beads, bound proteins were eluted and the GST fusion proteins were separated from co-eluting histones by SDS-PAGE (Figure 4B). Quantification of experimental triplicates revealed that GST-AD/VAA interacted ∼41% less efficiently with the histones than GST-AD/WT, while the interaction of GST-AD/EDD was ∼46% more efficiently than that of GST-AD/WT (Figure 4C). To directly assess the influence of CK2-mediated phosphorylation on the GST-AD interaction with histone H2A–H2B, GST-AD/WT was phospho-

A

DGSDSESGGSEESDKGYEPSDVEVESESEDEASESESLVESDDDEEEDSEQESEEEKGKTWDELEREATNADREHGVESDSEEE

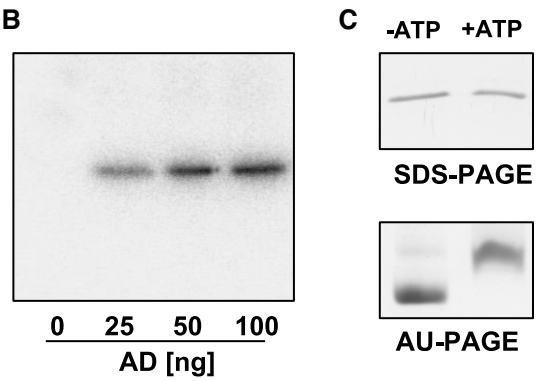

D

Modification	Experiment 1 # Spectra	Experiment 2 # Spectra
T1013P	0	1
T1023P	24	14
S1033P	68	40
S1035P	49	29
other P events	0	0

Figure 3. Protein kinase CK2 phosphorylates SPT16 within the acidic domain (AD). (**A**) Amino acid sequence of the acidic domain (AD, D955-R1075) of SPT16. Detected phosphosites (S1033, S1035 and T1023) in SPT16 isolated from *Arabidopsis* cells are indicated in red, while additional minimal CK2 consensus sites are indicated in blue. (**B**) Different amounts of SPT16-AD phosphorylated *in vitro* by recombinant maize CK2α in the presence of [γ-^{32}P]ATP after analysis by SDS-PAGE and phosphoimaging. (**C**) Reaction of SPT16-AD with CK2α in absence or presence of unlabelled ATP after separation by SDS-PAGE (top) or AU-PAGE (bottom) visualised by Coomassie staining. (**D**) SPT16-AD samples phosphorylated *in vitro* (as in C) were digested with trypsin and analysed by LC–MS/MS. Two replicates were analysed revealing phosphorylation events comparable to those detected *in vivo*.

rylated by CK2 *in vitro* prior to the binding assay, or mock-phosphorylated (no ATP added) (Figure 4D). Quantification of experimental triplicates demonstrated that CK2-phosphorylated GST-AD/WT interacted ∼44% more efficiently with the histones than the mock-phosphorylated protein (Figure 4E). The specificity of the AD-histone interaction is also evident from the lack of binding of H2A–H2B to unfused GST and the lack of binding of the small basic protein CytC to GST-AD/EDD in the GST pull-down assay (Figure 4F). Additionally, the histone interaction of the GST-AD variants was analysed in solution using microscale thermophoresis. The measurements confirmed the higher affinity for histones of GST-AD/EDD (K_d = 1.73 μM), while GST-AD/WT and GST-AD/VAA (K_d = 3.64 and 4.18 μM, respectively) bound similarly to the histones (Supplementary Figure S5).

To further evaluate the role of the AD of SPT16 in histone interactions, the wild-type version SPT16/WT-GS and for comparison mutated variants of SPT16 were expressed in *Arabidopsis* suspension cultured cells. In the mutated variants the three phosphorylatable S/T residues of the AD were replaced as above by non-phosphorylatable residues (termed SPT16/VAA) or by phosphomimicking residues (termed SPT16/EDD). IgG affinity purification from the different cell lines resulted in co-purification of SSRP1 with the three SPT16-GS versions (Figure 4G). Moreover, histones were clearly enriched in the eluates of the SPT16/WT-GS, SPT16/VAA-GS and SPT16/EDD-GS proteins, but not with the unfused GS control. The co-eluted histone bands were noticeably more prominent with SPT16/WT-GS and SPT16/EDD-GS when compared with SPT16/VAA-GS. This observation was confirmed by immunoblot analyses using antibodies directed against histones H2B and H3 (Figure 4H). Together these experiments suggest that the phosphorylation of SPT16 increases interaction with nucleosomal histones.

Role of SPT16 phosphorylation in plant growth and development

To study the possible involvement of the three identified SPT16 phosphorylation sites in plant development, we expressed wild type and mutant versions of SPT16 fused with the red fluorescent protein (TagRFP) in *spt16* T-DNA insertion plants under control of the *SPT16* promoter. Coding sequences were fused to the sequence encoding TagRFP to enable the detection of protein expression and localization. The expression constructs were introduced into *spt16-1* plants (Supplementary Figure S6A). This mutant allele expresses reduced levels of SPT16 (41) and immunoblot analyses of nuclear protein extracts using a SPT16-specific antibody revealed that the different SPT16-TagRFP fusion proteins are expressed in the different plant lines along with the endogenous SPT16 (Supplementary Figure S6B, C). CLSM confirmed the nuclear localization of SPT16-TagRFP and of the corresponding phospho-site variants in root tips (Supplementary Figure S6D). Phenotypic analyses of the *spt16* plants expressing the different SPT16 variants relative to the Col-0 wild-type control demonstrated that expression of SPT16 and the phosphomimic variant partially complemented the mutant phenotype, whereas the non-phosphorylatable variant hardly imparted complementation (Figure 5A). We analysed in detail some of the phenotypic characteristics that are clearly affected in *spt16* mutant plants (41). Thus, the early bolting phenotype of *spt16* is partially complemented by the expression of SPT16/WT and SPT16/EDD (resembling Col-0), whereas the bolting of the plants expressing SPT16/VAA is comparable to that of *spt16* (Figure 5B). The reduced rosette diameter of *spt16* is also more efficiently complemented by the expression of SPT16/WT and SPT16/EDD. Likewise, the increased number of primary inflorescences of *spt16* is reduced to a greater extent by the expression of SPT16/WT and SPT16/EDD relative to SPT16/VAA. The ability to complement mu-

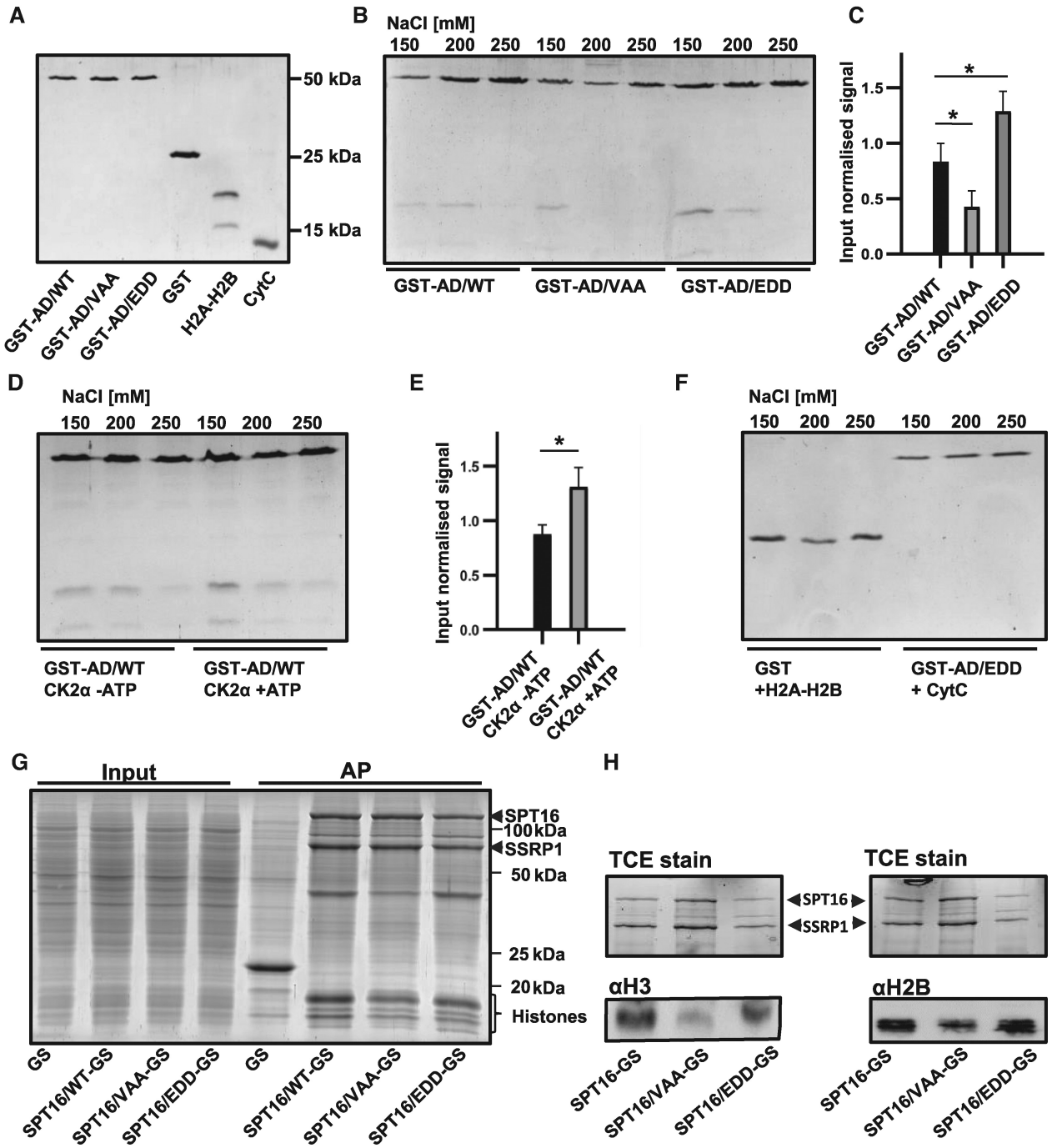

Figure 4. Phosphorylation of the SPT16 acidic domain modulates interactions with histones. (**A**) SDS-PAGE analysis of GST-AD/WT, GST-AD/VAA (with T1023V/S1033A/S1035A), GST-AD/EDD (with T1023E, S1033D, S1035D), unfused GST, recombinant *Arabidopsis* H2A–H2B and bovine Cytochrome C (CytC) visualised by Coomassie staining. (**B**) Comparative GST pull-down assays performed with GST-AD/WT, GST-AD/VAA and GST-AD/EDD, and with H2A–H2B in the presence of the indicated concentrations of NaCl. Eluted proteins were analysed by SDS-PAGE and Coomassie staining. (**C**) Quantification of H2B normalised to the GST-bait protein in presence of 150 mM NaCl. Statistical analysis of three replicates was performed using an unpaired t-test (p-value < 0.05). (**D**) Comparative GST pull-down assays performed with GST-AD/WT after phosphorylation with CK2α in absence/presence of ATP, respectively. (**E**) Quantification of H2B normalised to the GST-bait protein in presence of 150 mM NaCl. Statistical analysis of three replicates was performed using an unpaired t-test (*P*-value < 0.05). (**F**) Control assays showing either unfused GST in pull-down experiments with *Arabidopsis* H2A–H2B (left), or GST-AD/EDD with CytC (right) in presence of the indicated NaCl concentrations, reveal no interaction. (**G**) Input samples (Input) and eluates of IgG affinity purifications (AP) of *Arabidopsis* PSB-D cells expressing the unfused GS-tag, SPT16/WT-GS or the phosphositemutants SPT16/VAA-GS and SPT16/EDD-GS. Proteins were analysed by SDS-PAGE and Coomassie staining. (**H**) Immunoblot analyses (bottom) of eluates from the IgG affinity purification (as in **G**) probed with antibodies specific for histone H3 (left) and H2B (right), along with TCE stains (top) of the same SDS-PAGE gel that was used for the respective immunoblot analysis, serving as loading control. SPT16 and SSRP1 are highlighted by triangles. TCE: 2,2,2-trichlorethanol.

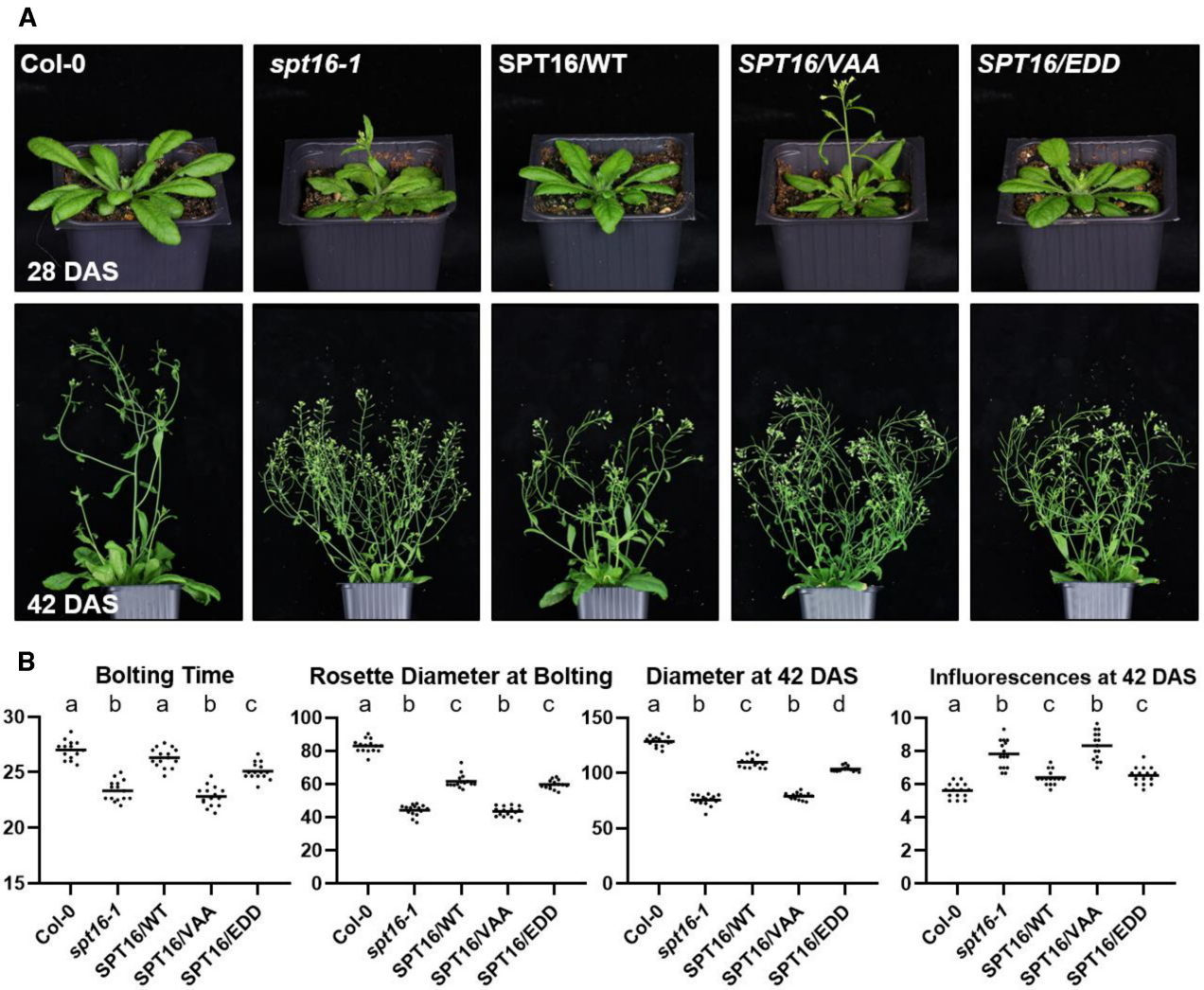

Figure 5. Phosphorylation of SPT16 acidic domain influences plant growth and development. Plants of the *spt16-1* mutant line were transformed with constructs driving the expression of wild-type SPT16 (termed SPT16/WT), the non-phosphorylatable (T1023V/S1033A/S1035A, termed SPT16/VAA) and phosphomimic (T1023E/S1033D/S1035D, termed SPT16/EDD) variants, and were phenotypically analysed relative to the wild-type (Col-0) and the *spt16-1* line. (**A**) Representative individuals of the different transgenic lines relative to Col-0 and *spt16-1* are shown at 28 DAS (top) and 42 DAS (bottom). (**B**) Quantification of phenotypic parameters. Day of bolting, rosette diameter at bolting [mm], rosette diameter at 42 DAS [mm], and number of primary inflorescences at 42 DAS were determined. Data comprised the measurements of 15 individual plants of each genotype in three biological replicates and was analysed by one-way ANOVA. The line in the scatterplot marks the average value and letters above the scatter indicate the outcome of the Tukey´s test (P-value < 0.05).

tant phenotypes also illustrated the functionality of the expressed SPT16 fusion proteins, which is in agreement with findings regarding SPT16 fusion proteins in other organisms (77,78). Thus, taken together the complementation analyses revealed that the expression of SPT16/VAA in *spt16* background resembles dominant-negative features and that phosphorylation of SPT16 is important for the impact of SPT16 on growth and development.

Effects on chromatin at transcriptional start sites

In view of the function of FACT as a histone chaperone and the distinct abilities of SPT16 and the corresponding phospho-site variants to complement the defects of *spt16* mutant plants, we examined possible alterations in the chromatin of the different genotypes. The genome-wide distribution of H3 was used as a proxi for nucleosome occupancy and compared using ChIPseq between the following genetic backgrounds, Col-0 wild-type, *spt16*, *spt16* expressing SPT16/WT, the non-phosphorylatable SPT16/VAA or the phosphomimic SPT16/EDD variants. Analysis of the ChIPseq data revealed that biological replicates of the analysed genotypes yielded robust results (Supplementary Figure S7). Consistent with previous studies on the genomic distribution of H3 in *Arabidopsis* (79,80), we observed in all genotypes an H3 enrichment over transposable elements (Supplementary Figure S8A) and a characteristically lower occupancy upstream of RNA polymerase II transcription start sites (TSSs) particularly of highly transcribed genes (Supplementary Figure S8B). The profiles of Col-0, *spt16* and *spt16* expressing the phosphomimic variant SPT16/EDD were comparable, whereas *spt16* expressing

the non-phosphorylatable variant SPT16/VAA showed a prominent H3 occupancy peak upstream of the TSS (peak centre ∼120 bp upstream of TSS), whose extent correlated with the transcript levels of the respective genes (Figure 6A). The H3 enrichment upstream of the TSS observed specifically for the *spt16* plants expressing the SPT16/VAA variant (Supplementary Figure S8C) is accompanied by lower H3 occupancy in the gene body (Figure 6B). The peak of H3 enrichment upstream of the TSS coincides with the position of nucleosome depleted regions and DNase hypersensitive sites reported in several studies analysing *Arabidopsis* chromatin (79–82). It is conceivable that nucleosome depletion upstream of the TSS is restricted in the presence of the non-phosphorylatable SPT16/VAA variant resulting in H3 accumulation. Therefore, H3 distribution was comparatively analysed for genes that showed a prominent H3 enrichment at the TSS (≥50% higher coverage in SPT16/VAA as compared to SPT16/WT, $P < 0.05$) in the presence of SPT16/VAA (384 genes) relative to genes, whose H3 occupancy was unchanged (3284 genes). While with the latter group of genes an essentially uniform H3 distribution was observed in all genotypes, the former group showed H3 enrichment upstream of the TSS that was strikingly enhanced in presence of the SPT16/VAA variant (Supplementary Figure S9). ChIP-qPCR analysis of the association of the SPT16 variants with the region upstream of the TSS of three loci that exhibit H3 enrichment revealed that SPT16 is detected, however, at levels clearly lower than within the transcribed region. No significant differences between the variants were observed (Supplementary Figure S10). Both in maize and *Arabidopsis*, nucleosomes were identified directly upstream of the TSS that proved particularly nuclease sensitive (69,83). The differential MNase digestion data obtained for *Arabidopsis* chromatin (69) were analysed comparatively for the two above-mentioned groups of genes. For both groups of genes, within the transcribed region high and low MNase digestion similarly revealed the characteristic nucleosomal pattern, albeit a more intense peak of the +1 nucleosome was observed for the genes with H3 enrichment upstream of the TSS upon expression of the SPT16/VAA variant (Supplementary Figure S11). However, MNase digestion of these genes varied markedly upstream of the TSS (left panel), whereas a much smaller difference between high and low digestion occurred with the group of genes with unchanged H3 distribution (right panel). There is a prominent peak at the position of the -1 nucleosome upon low MNase digestion that is substantially weaker upon high MNase digestion (indicative of an unstable/fragile nucleosome) specifically with the group of genes showing H3 accumulation upstream of the TSS in the presence of the non-phosphorylatable SPT16/VAA. Centring H3 ChIPseq tracks and MNase-seq tracks over the TSSs of all protein-coding genes clarified the correlation of H3 enrichment observed with SPT16/VAA and of the region of most pronounced variability in MNase accessibility (Supplementary Figure S12). The H3 occupancy based on the ChIPseq analysis plotted in comparison to the differential MNase digestion (69) at individual loci illustrates these effects (Figure 6C). Here it is evident that the H3 enrichment upstream of the TSS observed in the presence of the non-phosphorylatable SPT16/VAA variant (but not with SPT16/WT or SPT16/EDD) coincides with the peak of an unstable/fragile nucleosome that is preferentially detected after low rather than high MNase digestion. In conclusion, these experiments suggest that at a subgroup of RNAPII-transcribed genes phosphorylation of SPT16 is required for establishing the correct nucleosome occupancy at the TSS.

DISCUSSION

Histone chaperones assist transcription of nucleosomal templates and concurrently maintain proper chromatin signature over transcribed genes. A prominent representative is the FACT heterodimer consisting of SSRP1 and SPT16 that promotes RNAPII progression through chromatin and assists other DNA-dependent processes. We identified post-translational modifications that may modulate the activity of FACT in *Arabidopsis* cells. Our analyses did not reveal a major role for the four acetylation sites that were mapped within the C-terminal region of SSRP1 comprising the HMG-box domain and the adjacent basic region. However, our study showed that three *in vivo* phosphorylation sites identified in the acidic domain of SPT16 impact deeply the function of FACT and its role in growth and development of *Arabidopsis*. The same three sites (and additional sites) were phosphorylated by protein kinase CK2 *in vitro*, suggesting that CK2 is the enzyme catalysing the phosphorylation *in planta*. In agreement with that several α and β subunits of the heterodimeric protein kinase CK2 family co-purified with the *Arabidopsis* RNAPII transcript elongation complex (45), similar to the situation in yeast (84). Comparing the amino acid sequences of the *Arabidopsis* SPT16 acidic domain with those of SPT16 proteins of other organisms revealed multiple CK2 consensus phosphorylation sites in all SPT16 proteins (Supplementary Figure S13). Phosphorylation of several residues within the acidic domain was also observed, when human SPT16 was isolated from insect cells (23). Therefore, CK2-mediated phosphorylation of SPT16 might be a common mechanism, as it has been described for SSRP1 (49–52). Since members of the plant CK2 family have been implicated in multiple developmental and stress-responsive pathways (85,86), it will be attractive to investigate whether phosphorylation of FACT plays a role in these processes.

In comparison to the wild-type acidic domain, the phosphomimic variant of the acidic domain (AD/EDD) bound *in vitro* more tightly to H2A–H2B heterodimers. Likewise, SPT16/WT and SPT16/EDD co-purified more efficiently with histones from *Arabidopsis* cells, when compared with the non-phosphorylatable SPT16/VAA variant. Therefore, the phosphorylatable SPT16/WT and phosphomimic SPT16/EDD variants interact efficiently with histones, whereas the histone-interactions of the non-phosphorylatable SPT16/VAA variant are reduced. The acidic region of SPT16 (and SSRP1) substantially contribute to the interaction with histones and are required for the nucleosome reorganizing function of FACT (22,24,26,27). CK2-mediated phosphorylation of the acidic region of SPT16 (and SSRP1) could fine-tune the interaction of FACT with nucleosomes. In line with that the phosphorylation of the acidic region of human SPT16 is cru-

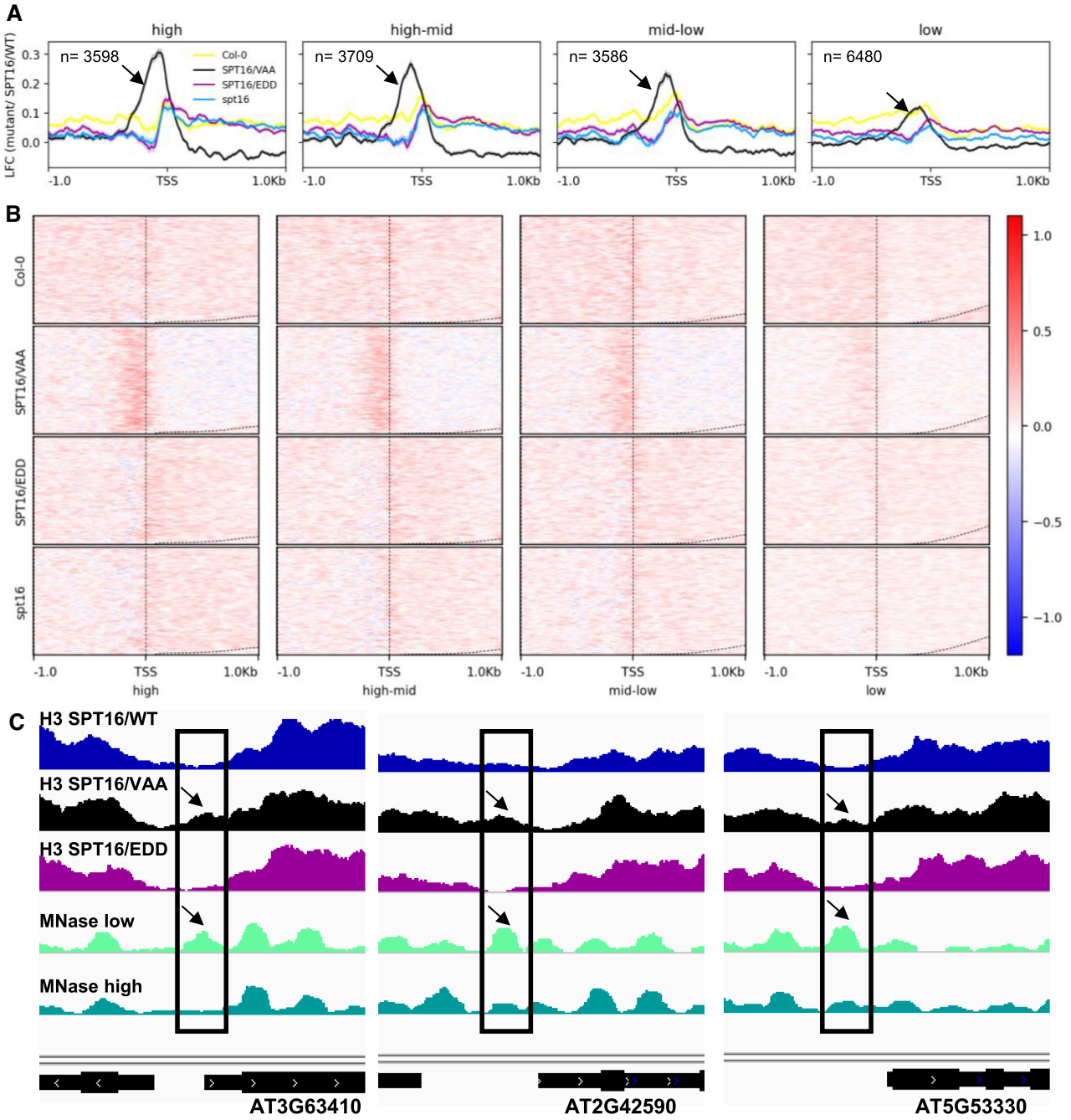

Figure 6. Enrichment of histone H3 in the presence of the non-phosphorylatable SPT16/VAA upstream of the TSS dependent on transcription. (**A**) Metagene plots (LFC, log-fold change) of H3 ChIPseq data (10-bp bins) in Col-0, *spt16* and *spt16* expressing SPT16/VAA or SPT16/EDD normalised to those expressing SPT16/WT. Mean signals of the biological replicates were averaged (line) and the tracks represent the SEM for the three replicates at each position (shaded area). The tracks are centred around the TSS and the panels represent non-overlapping protein-coding genes grouped according to transcript levels (high, high-mid, mid-low, low) based on RNAseq data obtained with 6 DAS Col-0 plants. Arrows indicate the transcription dependent peak of H3 enrichment in SPT16/VAA expressing plants. (**B**) Heatmaps illustrating the distribution of H3 in the different plants lines. H3 occupancy is normalised to the plants expressing SPT16/WT and genes in the different panels are grouped related to transcript levels as above. The relative H3 occupancy is colour coded as indicated. (**C**) H3 enrichment upstream of the TSS in presence of SPT16/VAA coincides with differential MNase peaks. Representative examples of H3 ChIPseq profiles representing a 1-kb region around the TSS were aligned with differential MNase (high/low MNase) sequencing data (69). Black boxes indicate a 150-bp window, while the arrows indicate an H3 peak occurring in *spt16* plants expressing the SPT16/VAA variant and a nucleosomal peak that preferentially is observed upon low MNase digestion. Gene models are shown at the bottom.

cial for the interaction with histones of a 112-bp octasome (23). Expression of the varying SPT16 variants in *spt16* plants complemented mutant phenotypes to different extents. SPT16/WT and SPT16/EDD complemented rather efficiently, for instance, the early bolting or increased number of primary inflorescences of *spt16* plants. In contrast, the SPT16/VAA variant proved inactive in reversing the mutant phenotype of *spt16* plants. This demonstrates that the phosphorylation of the SPT16 acidic domain is important for the *in vivo* functionality of FACT.

Analysis of the genomic distribution of histone H3 revealed that mutation of phosphorylation sites in the FACT subunit SPT16 impacted on nucleosome occupancy upstream of the TSS. In presence of the non-phosphorylatable SPT16/VAA variant a peak of H3 enrichment was detected particularly with highly transcribed genes. In contrast to that H3 distribution of plants expressing the phosphorylatable SPT16/WT and the phosphomimic SPT16/EDD variants resembled that of wild-type plants. As expected the association of the SPT16 variants with the regions upstream of the TSSs did not differ significantly. We rather think that SPT16 is phosphorylated by CK2 after FACT recruitment to chromatin. Although both FACT and CK2 associate with the RNAPII elongation complex, their occupancy in chromatin could differ and co-localization of FACT and CK2 may define SPT16 phosphorylation-regulated genomic target sites. The genomic region of the SPT16/VAA-specific H3 enrichment corresponds with a position in *Arabidopsis* chromatin that is characterised as nucleosome depleted region and DNase hypersensitive site (79–82). Increased histone occupancy upstream of the TSS occurred also in yeast cells upon SPT16 depletion (87). Interestingly, the site of H3 enrichment in presence of the non-phosphorylatable SPT16/VAA variant is in accordance with a notable differentially MNase sensitive peak that most likely represents unstable/fragile -1 nucleosomes (69) occurring also in yeast and metazoan chromatin (88–90). In our analyses, this feature correlated with high transcript levels and also in yeast unstable/fragile -1 nucleosomes are linked to transcriptional activity (88). One should expect that H3 enrichment related to persistence of an (unstable/fragile) nucleosome upstream of the TSS interferes with binding of transcription factors and/or RNAPII recruitment, and hence leads to mis-regulation and/or reduced transcriptional output. The role of unstable/fragile nucleosomes currently has not been clarified in plant transcription. In yeast, these unstable nucleosomes are proposed to contribute to poising genes for transcription (91), which is also conceivable in plants (69). Although our ChIPseq analysis convincingly demonstrated distinct H3 accumulation upstream of the TSS at 384 genes, we still expect that the magnitude of the effect is underestimated from our experiments primarily for two reasons: (i) we have mutated three amino acid residues within the acidic domain of SPT16 that were confirmed phosphorylation sites, but as detailed above there are several additional CK2 consensus sites that quite possibly are phosphorylated *in planta* and likely could increase phosphorylation-dependent impact. (ii) The mutated and wild-type SPT16 expression constructs were introduced into the *spt16-1* mutant line, in which SPT16 levels are reduced to <50% (41), but the mutant plants still contain wild-type SPT16 that may mask the effects of the introduced SPT16 variants.

In yeast, the abundant histone chaperones FACT and SPT6 collaborate in managing nucleosomes (87,92) and the activity of SPT6 is also under control of CK2-catalysed phosphorylation (93). The *Arabidopsis* orthologue SPT6L can be recruited to the TSS independent of RNAPII and plays a role during early transcription (94). Therefore, it is conceivable that FACT and SPT6L jointly regulate early transcriptional elongation in plants, since both histone chaperones and the protein kinase associate with RNAPII (45,84). Our identification of CK2-mediated phosphorylation of SPT16 and its implication on nucleosome occupancy at TSSs as well as its influence on plant development paved the way for further studies addressing the interplay of histone chaperones and CK2 in the regulation of chromatin dynamics in the *Arabidopsis* model.

DATA AVAILABILITY

The ChIPseq data have been deposited to the NCBI sequence read archive with the accession code PRJNA748845, while mass spectrometry data have been deposited to the PRIDE database with the accession code PXD028534.

SUPPLEMENTARY DATA

Supplementary Data are available at NAR Online.

ACKNOWLEDGEMENTS

We thank Ina Weig-Meckl for performing qPCR analyses, Klaus Tiefenbach for assistance in recording CD spectra, Tina Ravnsborg for help analysing MS data, and the Nottingham Arabidopsis Stock Centre (NASC) for providing *Arabidopsis* T-DNA insertion lines.

FUNDING

German Research Foundation (DFG) [Gr1159/14-2 and SFB960/A6 to K.D.G.]; proteomics and mass spectrometry research at SDU is supported by generous grants to the VILLUM Center for Bioanalytical Sciences (VILLUM Foundation) [7292 to O.N.J., PRO-MS]; Danish National Mass Spectrometry Platform for Functional Proteomics [5072-00007B to O.N.J.]; Danish National Research Foundation Center for Epigenetics [DNRF 82]. Funding for open access charge: DFG.
Conflict of interest statement. None declared.

REFERENCES

1. Kornberg,R.D. and Lorch,Y. (2020) Primary role of the nucleosome. *Mol. Cell*, **79**, 371–375.
2. Li,B., Carey,M. and Workman,J.L. (2007) The role of chromatin during transcription. *Cell*, **128**, 707–719.
3. Kujirai,T. and Kurumizaka,H. (2020) Transcription through the nucleosome. *Curr. Opin. Struct. Biol.*, **61**, 42–49.
4. Das,C., Tyler,J.K. and Churchill,M.E.A. (2010) The histone shuffle: histone chaperones in an energetic dance. *Trends Biochem. Sci.*, **35**, 476–489.

5. Gurard-Levin,Z.A., Quivy,J.-P. and Almouzni,G. (2014) Histone chaperones: assisting histone traffic and nucleosome dynamics. *Ann. Rev. Biochem.*, **83**, 487–517.
6. Hammond,C.M., Strømme,C.B., Huang,H., Patel,D.J. and Groth,A. (2017) Histone chaperone networks shaping chromatin function. *Nat. Rev. Mol. Cell Biol.*, **18**, 141–158.
7. Brewster,N.K., Johnston,G.C. and Singer,R.A. (1998) Characterization of the CP complex, an abundant dimer of Cdc68 and Pob3 proteins that regulates yeast transcriptional activation and chromatin repression. *J. Biol. Chem.*, **273**, 21972–21979.
8. Orphanides,G., LeRoy,G., Chang,C.-H., Luse,D.S. and Reinberg,D. (1998) FACT, a factor that facilitates transcript elongation through nucleosomes. *Cell*, **92**, 105–116.
9. Orphanides,G., Wu,W.H., Lane,W.S., Hampsey,M. and Reinberg,D. (1999) The chromatin-specific transcription elongation factor FACT comprises human SPT16 and SSRP1 proteins. *Nature*, **400**, 284–288.
10. Wittmeyer,J., Joss,L. and Formosa,T. (1999) Spt16 and Pob3 of *Saccharomyces cerevisiae* form an essential, abundant heterodimer that is nuclear, chromatin-associated, and copurifies with DNA polymerase alpha. *Biochemistry*, **38**, 8961–8971.
11. Formosa,T. and Winston,F. (2020) The role of FACT in managing chromatin: disruption, assembly, or repair?*Nucleic Acids Res.*, **48**, 11929–11941.
12. Gurova,K., Chang,H.-W., Valieva,M.E., Sandlesh,P. and Studitsky,V.M. (2018) Structure and function of the histone chaperone FACT - Resolving FACTual issues. *Biochim. Biophys. Acta*, **1861**, 892–904.
13. Belotserkovskaya,R. and Reinberg,D. (2004) Facts about FACT and transcript elongation through chromatin. *Curr. Opin. Genet. Dev.*, **14**, 139–146.
14. Zhou,K., Liu,Y. and Luger,K. (2020) Histone chaperone FACT FAcilitates Chromatin Transcription: mechanistic and structural insights. *Curr. Opin. Struct. Biol.*, **65**, 26–32.
15. Malone,E.A., Clark,C.D., Chiang,A. and Winston,F. (1991) Mutations in SPT16/CDC68 suppress cis- and trans-acting mutations that affect promoter function in Saccharomyces cerevisiae. *Mol. Cell. Biol.*, **11**, 5710–5717.
16. Ransom,M., Williams,S.K., Dechassa,M.L., Das,C., Linger,J., Adkins,M., Liu,C., Bartholomew,B. and Tyler,J.K. (2009) FACT and the proteasome promote promoter chromatin disassembly and transcriptional initiation. *J. Biol. Chem.*, **284**, 23461–23471.
17. Petrenko,N., Jin,Y., Dong,L., Wong,K.H. and Struhl,K. (2019) Requirements for RNA polymerase II preinitiation complex formation in vivo. *Elife*, **8**, e43654.
18. Yu,Y., Yarrington,R.M. and Stillman,D.J. (2020) FACT and Ash1 promote long-range and bidirectional nucleosome eviction at the HO promoter. *Nucleic. Acids. Res.*, **48**, 10877–10889.
19. Belotserkovskaya,R., Oh,S., Bondarenko,V.A., Orphanides,G., Studitsky,V.M. and Reinberg,D. (2003) FACT facilitates transcription-dependent nucleosome alteration. *Science*, **301**, 1090–1093.
20. Hsieh,F.-K., Kulaeva,O.I., Patel,S.S., Dyer,P.N., Luger,K., Reinberg,D. and Studitsky,V.M. (2013) Histone chaperone FACT action during transcription through chromatin by RNA polymerase II. *Proc. Natl. Acad. Sci. U.S.A.*, **110**, 7654–7659.
21. Hondele,M., Stuwe,T., Hassler,M., Halbach,F., Bowman,A., Zhang,E.T., Nijmeijer,B., Kotthoff,C., Rybin,V., Amlacher,S. *et al.* (2013) Structural basis of histone H2A–H2B recognition by the essential chaperone FACT. *Nature*, **499**, 111–114.
22. Kemble,D.J., McCullough,L.L., Whitby,F.G., Formosa,T. and Hill,C.P. (2015) FACT disrupts nucleosome structure by binding H2A–H2B with conserved peptide motifs. *Mol. Cell*, **60**, 294–306.
23. Mayanagi,K., Saikusa,K., Miyazaki,N., Akashi,S., Iwasaki,K., Nishimura,Y., Morikawa,K. and Tsunaka,Y. (2019) Structural visualization of key steps in nucleosome reorganization by human FACT. *Sci. Rep.*, **9**, 10183.
24. Tsunaka,Y., Fujiwara,Y., Oyama,T., Hirose,S. and Morikawa,K. (2016) Integrated molecular mechanism directing nucleosome reorganization by human FACT. *Genes Dev.*, **30**, 673–686.
25. Wang,T., Liu,Y., Edwards,G., Krzizike,D., Scherman,H. and Luger,K. (2018) The histone chaperone FACT modulates nucleosome structure by tethering its components. *Life Sci. Alliance*, **1**, e201800107.
26. Winkler,D.D., Muthurajan,U.M., Hieb,A.R. and Luger,K. (2011) Histone chaperone FACT coordinates nucleosome interaction through multiple synergistic binding events. *J. Biol. Chem.*, **286**, 41883–41892.
27. Liu,Y., Zhou,K., Zhang,N., Wei,H., Tan,Y.Z., Zhang,Z., Carragher,B., Potter,C.S., D'Arcy,S. and Luger,K. (2020) FACT caught in the act of manipulating the nucleosome. *Nature*, **577**, 426–431.
28. Xin,H., Takahata,S., Blanksma,M., McCullough,L., Stillman,D.J. and Formosa,T. (2009) yFACT induces global accessibility of nucleosomal DNA without H2A–H2B displacement. *Mol. Cell*, **35**, 365–376.
29. Valieva,M.E., Armeev,G.A., Kudryashova,K.S., Gerasimova,N.S., Shaytan,A.K., Kulaeva,O.I., McCullough,L.L., Formosa,T., Georgiev,P.G., Kirpichnikov,M.P. *et al.* (2016) Large-scale ATP-independent nucleosome unfolding by a histone chaperone. *Nat. Struct. Mol. Biol.*, **23**, 1111–1116.
30. Kaplan,C.D., Laprade,L. and Winston,F. (2003) Transcription elongation factors repress transcription initiation from cryptic sites. *Science*, **301**, 1096–1099.
31. Mason,P.B. and Struhl,K. (2003) The FACT complex travels with elongating RNA polymerase II and is important for the fidelity of transcriptional initiation in vivo. *Mol. Cell. Biol.*, **23**, 8323–8333.
32. Cheung,V., Chua,G., Batada,N.N., Landry,C.R., Michnick,S.W., Hughes,T.R. and Winston,F. (2008) Chromatin- and transcription-related factors repress transcription from within coding regions throughout the Saccharomyces cerevisiae genome. *PLoS Biol.*, **6**, e277.
33. Kumar,A. and Vasudevan,D. (2020) Structure-function relationship of H2A–H2B specific plant histone chaperones. *Cell Stress Chaperones*, **25**, 1–17.
34. Tripathi,A.K., Singh,K., Pareek,A. and Singla-Pareek,S.L. (2015) Histone chaperones in *Arabidopsis* and rice: genome-wide identification, phylogeny, architecture and transcriptional regulation. *BMC Plant Biol.*, **15**, 42.
35. Zhu,Y., Dong,A. and Shen,W.H. (2013) Histone variants and chromatin assembly in plant abiotic stress responses. *Biochim. Biophys. Acta*, **1819**, 343–348.
36. Probst,A.V. and Mittelsten Scheid,O. (2015) Stress-induced structural changes in plant chromatin. *Curr. Opin. Plant Biol.*, **27**, 8–16.
37. Otero,S., Desvoyes,B. and Gutierrez,C. (2014) Histone H3 dynamics in plant cell cycle and development. *Cytogenet. Genome Res.*, **143**, 114–124.
38. Grasser,K.D. (2020) The FACT histone chaperone: tuning gene transcription in the chromatin context to modulate plant growth and development. *Front. Plant Sci.*, **11**, 85.
39. Zhou,W., Zhu,Y., Dong,A. and Shen,W.-H. (2015) Histone H2A/H2B chaperones: from molecules to chromatin-based functions in plant growth and development. *Plant J.*, **83**, 78–95.
40. Frost,J.M., Kim,M.Y., Park,G.T., Hsieh,P.H., Nakamura,M., Lin,S.J.H., Yoo,H., Choi,J., Ikeda,Y., Kinoshita,T. *et al.* (2018) *Arabidopsis*. *Proc. Natl. Acad. Sci. U.S.A.*, **115**, E4720–E4729.
41. Lolas,I.B., Himanen,K., Grønlund,J.T., Lynggaard,C., Houben,A., Melzer,M., van Lijsebettens,M. and Grasser,K.D. (2010) The transcript elongation factor FACT affects *Arabidopsis* vegetative and reproductive development and genetically interacts with *HUB1/2*. *Plant J.*, **61**, 686–697.
42. Duroux,M., Houben,A., Ruzicka,K., Friml,J. and Grasser,K.D. (2004) The chromatin remodelling complex FACT associates with actively transcribed regions of the *Arabidopsis* genome. *Plant J.*, **40**, 660–671.
43. Ikeda,Y., Kinoshita,Y., Susaki,D., Iwano,M., Takayama,S., Higashiyama,T., Kakutani,T. and Kinoshita,T. (2011) HMG domain containing SSRP1 is required for DNA demethylation and genomic imprinting in *Arabidopsis*. *Dev. Cell*, **21**, 589–596.
44. Pfab,A., Breindl,M. and Grasser,K.D. (2018) The *Arabidopsis* histone chaperone FACT is required for stress-induced expression of anthocyanin biosynthetic genes. *Plant Mol. Biol.*, **96**, 367–374.
45. Antosz,W., Pfab,A., Ehrnsberger,H.F., Holzinger,P., Köllen,K., Mortensen,S.A., Bruckmann,A., Schubert,T., Längst,G., Griesenbeck,J. *et al.* (2017) Composition of the *Arabidopsis* RNA polymerase II transcript elongation complex reveals the interplay between elongation and mRNA processing factors. *Plant Cell*, **29**, 854–870.

46. Ma,Y., Gil,S., Grasser,K.D. and Mas,P. (2018) Targeted recruitment of the basal transcriptional machinery by LNK clock components controls the circadian rhythms of nascent RNAs in *Arabidopsis*. *Plant Cell*, **30**, 907–924.
47. Perales,M. and Más,P. (2007) A functional link between rhythmic changes in chromatin structure and the *Arabidopsis* biological clock. *Plant Cell*, **19**, 2111–2123.
48. Nielsen,M., Ard,R., Leng,X., Ivanov,M., Kindgren,P., Pelechano,V. and Marquardt,S. (2019) Transcription-driven chromatin repression of Intragenic transcription start sites. *PLoS Genet.*, **15**, e1007969.
49. Krohn,N.M., Stemmer,C., Fojan,P., Grimm,R. and Grasser,K.D. (2003) Protein kinase CK2 phosphorylates the high mobility group domain protein SSRP1, inducing the recognition of UV-damaged DNA. *J. Biol. Chem.*, **278**, 12710–12715.
50. Li,Y., Keller,D.M., Scott,J.D. and Lu,H. (2005) CK2 phosphorylates SSRP1 and inhibits its DNA-binding activity. *J. Biol. Chem.*, **280**, 11869–11875.
51. Aoki,D., Awazu,A., Fujii,M., Uewaki,J.I., Hashimoto,M., Tochio,N., Umehara,T. and Tate,S.I. (2020) Ultrasensitive change in nucleosome binding by multiple phosphorylations to the intrinsically disordered region of the histone chaperone FACT. *J. Mol. Biol.*, **432**, 4637–4657.
52. Tsunaka,Y., Toga,J., Yamaguchi,H., Tate,S., Hirose,S. and Morikawa,K. (2009) Phosphorylated intrinsically disordered region of FACT masks its nucleosomal DNA binding elements. *J. Biol. Chem.*, **284**, 24610–24621.
53. Dürr,J., Lolas,I.B., Sørensen,B.B., Schubert,V., Houben,A., Melzer,M., Deutzmann,R., Grasser,M. and Grasser,K.D. (2014) The transcript elongation factor SPT4/SPT5 is involved in auxin-related gene expression in *Arabidopsis*. *Nucleic Acids Res.*, **42**, 4332–4347.
54. Pfab,A., Grønlund,J.T., Holzinger,P., Längst,G. and Grasser,K.D. (2018) The *Arabidopsis* histone chaperone FACT: role of the HMG-box domain of SSRP1. *J. Mol. Biol.*, **430**, 2747–2759.
55. Zhou,J., Applegate,C., Alonso,A.D., Reynolds,D., Orford,S., Mackiewicz,M., Griffiths,S., Penfield,S. and Pullen,N. (2017) Leaf-GP: an open and automated software application for measuring growth phenotypes for Arabidopsis and wheat. *Plant Meth.*, **13**, 117.
56. van Leene,J., Eeckhout,D., Cannoot,B., Winne,N., Persiau,G., van de Slijke,E., Vercruysse,L., Dedecker,M., Vandepoele,K., Martens,L. *et al.* (2015) An improved toolbox to unravel the plant cellular machinery by tandem affinity purification of *Arabidopsis* protein complexes. *Nat. Protoc.*, **10**, 169–187.
57. Kovalchuk,S.I., Jensen,O.N. and Rogowska-Wrzesinska,A. (2019) FlashPack: fast and simple preparation of ultrahigh-performance capillary columns for LC-MS. *Mol. Cell. Proteomics*, **18**, 383–390.
58. Antosz,W., Deforges,J., Begcy,K., Bruckmann,A., Poirier,Y., Dresselhaus,T. and Grasser,K.D. (2020) Critical role of transcript cleavage in Arabidopsis RNA polymerase II transcriptional elongation. *Plant Cell*, **32**, 1449–1463.
59. Ritt,C., Grimm,R., Fernandez,S., Alonso,J.C. and Grasser,K.D. (1998) Basic and acidic regions flanking the HMG domain of maize HMGa modulate the interactions with DNA and the self-association of the protein. *Biochemistry*, **37**, 2673–2681.
60. Osakabe,A., Lorkovic,Z.J., Kobayashi,W., Tachiwana,H., Yelagandula,R., Kurumizaka,H. and Berger,F. (2018) Histone H2A variants confer specific properties to nucleosomes and impact on chromatin accessibility. *Nucleic. Acids. Res.*, **46**, 7675–7685.
61. Luger,K., Rechsteiner,T.J. and Richmond,T.J. (1999) Expression and purification of recombinant histones and nucleosome reconstitution. *Methods Mol. Biol.*, **119**, 1–16.
62. Stemmer,C., Schwander,A., Bauw,G., Fojan,P. and Grasser,K.D. (2002) Protein kinase CK2 differentially phosphorylates maize chromosomal high mobility group B (HMGB) proteins modulating their stability and DNA interactions. *J. Biol. Chem.*, **277**, 1092–1098.
63. Myers,J.K., Pace,C.N. and Scholtz,J.M. (1997) Helix propensities are identical in proteins and peptides. *Biochemistry*, **36**, 10923–10929.
64. Shechter,D., Dormann,H.L., Allis,C.D. and Hake,S.B. (2007) Extraction, purification and analysis of histones. *Nat. Protoc.*, **2**, 1445–1457.
65. Langmead,B. and Salzberg,S.L. (2012) Fast gapped-read alignment with Bowtie 2. *Nat. Meth.*, **9**, 357–359.
66. Chen,K., Xi,Y., Pan,X., Li,Z., Kaestner,K., Tyler,J., Dent,S., He,X. and Li,W. (2013) DANPOS: dynamic analysis of nucleosome position and occupancy by sequencing. *Genome Res.*, **23**, 341–351.
67. Ramírez,F., Ryan,D.P., Grüning,B., Bhardwaj,V., Kilpert,F., Richter,A.S., Heyne,S., Dündar,F. and Manke,T. (2016) deepTools2: a next generation web server for deep-sequencing data analysis. *Nucleic Acids Res.*, **44**, W160–W165.
68. Ewels,P., Magnusson,M., Lundin,S. and Käller,M. (2016) MultiQC: summarize analysis results for multiple tools and samples in a single report. *Bioinformatics*, **32**, 3047–3048.
69. Pass,D.A., Sornay,E., Marchbank,A., Crawford,M.R., Paszkiewicz,K., Kent,N.A. and Murray,J.A.H. (2017) Genome-wide chromatin mapping with size resolution reveals a dynamic sub-nucleosomal landscape in Arabidopsis. *PLoS Genet.*, **13**, e1006988.
70. Assenberg,R., Webb,M., Connolly,E., Stott,K., Watson,M., Hobbs,J. and Thomas,J.O. (2008) A critical role in structure-specific DNA binding for the acetylatable lysine residues in HMGB1. *Biochem. J.*, **411**, 553–561.
71. Pelletier,G., Stefanovsky,V.Y., Faubladier,M., Hirschler-Lazkiewicz,I., Savard,J., Rothblum,L.I., Côté,J. and Moss,T. (2000) Competitive recruitment of CBP and Rb-HDAC regulates UBF acetylation and ribosomal transcription. *Mol. Cell*, **6**, 1059–1066.
72. Malarkey,C.S. and Churchill,M.E. (2012) The high mobility group box: the ultimate utility player of a cell. *Trends Biochem. Sci.*, **37**, 553–562.
73. Antosch,M., Mortensen,S.A. and Grasser,K.D. (2012) Plant proteins containing high mobility group box DNA-binding domains modulate different nuclear processes. *Plant Physiol.*, **159**, 875–883.
74. Bonaldi,T., Talamo,F., Scaffidi,P., Ferrera,D., Porto,A., Bachi,A., Rubartelli,A., Agresti,A. and Bianchi,M.E. (2003) Monocytic cells hyperacetylate chromatin protein HMGB1 to redirect it towards secretion. *EMBO J.*, **22**, 5551–5560.
75. Röttgers,K., Krohn,N.M., Lichota,J., Stemmer,C., Merkle,T. and Grasser,K.D. (2000) DNA-interactions and nuclear localisation of the chromosomal HMG domain protein SSRP1 from maize. *Plant J.*, **23**, 395–405.
76. Litchfield,D.W. (2003) Protein kinase CK2: structure, regulation and role in cellular decisions of life and death. *Biochem. J.*, **369**, 1–15.
77. Wienholz,F., Zhou,Di, Turkyilmaz,Y., Schwertman,P., Tresini,M., Pines,A., van Toorn,M., Bezstarosti,K., Demmers,J.A.A. and Marteijn,J.A. (2019) FACT subunit Spt16 controls UVSSA recruitment to lesion-stalled RNA Pol II and stimulates TC-NER. *Nucleic Acids Res.*, **47**, 4011–4025.
78. Vanssay,A., Touzeau,A., Arnaiz,O., Frapporti,A., Phipps,J. and Duharcourt,S. (2020) The Paramecium histone chaperone Spt16-1 is required for Pgm endonuclease function in programmed genome rearrangements. *PLoS Genet.*, **16**, e1008949.
79. Stroud,H., Otero,S., Desvoyes,B., Ramirez-Parra,E., Jacobsen,S.E. and Gutierrez,C. (2012) Genome-wide analysis of histone H3.1 and H3.3 variants in *Arabidopsis thaliana*. *Proc. Natl. Acad. Sci. U.S.A.*, **109**, 5370–5375.
80. Zhang,T., Zhang,W. and Jiang,J. (2015) Genome-wide nucleosome occupancy and positioning and their impact on gene expression and evolution in plants. *Plant Physiol.*, **168**, 1406–1416.
81. Liu,M.-J., Seddon,A.E., Tsai,Z.T.-Y., Major,I.T., Floer,M., Howe,G.A. and Shiu,S.-H. (2015) Determinants of nucleosome positioning and their influence on plant gene expression. *Genome Res.*, **25**, 1182–1195.
82. Zhang,W., Zhang,T., Wu,Y. and Jiang,J. (2012) Genome-wide identification of regulatory DNA elements and protein-binding footprints using signatures of open chromatin in Arabidopsis. *Plant Cell*, **24**, 2719–2731.
83. Vera,D.L., Madzima,T.F., Labonne,J.D., Alam,M.P., Hoffman,G.G., Girimurugan,S.B., Zhang,J., McGinnis,K.M., Dennis,J.H. and Bass,H.W. (2014) Differential nuclease sensitivity profiling of chromatin reveals biochemical footprints coupled to gene expression and functional DNA elements in maize. *Plant Cell*, **26**, 3883–3893.
84. Krogan,N.J., Kim,M., Ahn,S.H., Zhong,G., Kobor,M.S., Cagney,G., Emili,A., Shilatifard,A., Buratowski,S. and Greenblatt,J.F. (2002) RNA polymerase II elongation factors of *Saccharomyces cerevisiae*: a targeted proteomics approach. *Mol.Cell.Biol.*, **22**, 6979–6992.
85. Vilela,B., Pagès,M. and Riera,M. (2015) Emerging roles of protein kinase CK2 in abscisic acid signaling. *Front. Plant Sci.*, **6**, 966.

86. Mulekar,J.J. and Huq,E. (2014) Expanding roles of protein kinase CK2 in regulating plant growth and development. *J. Exp. Bot.*, **65**, 2883–2893.
87. Jeronimo,C., Poitras,C. and Robert,F. (2019) Histone recycling by FACT and Spt6 during transcription prevents the scrambling of histone modifications. *Cell Rep.*, **28**, 1206–1218.
88. Kubik,S., Bruzzone,M.J. and Shore,D. (2017) Establishing nucleosome architecture and stability at promoters: roles of pioneer transcription factors and the RSC chromatin remodeler. *Bioessays*, **39**, 1600237.
89. Mieczkowski,J., Cook,A., Bowman,S.K., Mueller,B., Alver,B.H., Kundu,S., Deaton,A.M., Urban,J.A., Larschan,E., Park,P.J. *et al.* (2016) MNase titration reveals differences between nucleosome occupancy and chromatin accessibility. *Nat. Commun.*, **7**, 11485.
90. Schwartz,U., Németh,A., Diermeier,S., Exler,J.H., Hansch,S., Maldonado,R., Heizinger,L., Merkl,R. and Längst,G. (2019) Characterizing the nuclease accessibility of DNA in human cells to map higher order structures of chromatin. *Nucleic Acids Res.*, **47**, 1239–1254.
91. Xi,Y., Yao,J., Chen,R., Li,W. and He,X. (2011) Nucleosome fragility reveals novel functional states of chromatin and poises genes for activation. *Genome Res.*, **21**, 718–724.
92. McCullough,L., Connell,Z., Petersen,C. and Formosa,T. (2015) The abundant histone chaperones Spt6 and FACT collaborate to assemble, inspect, and maintain chromatin structure in *Saccharomyces cerevisiae*. *Genetics*, **201**, 1031–1045.
93. Gouot,E., Bhat,W., Rufiange,A., Fournier,E., Paquet,E. and Nourani,A. (2018) Casein kinase 2 mediated phosphorylation of Spt6 modulates histone dynamics and regulates spurious transcription. *Nucleic Acids Res.*, **46**, 7612–7630.
94. Chen,C., Shu,J., Li,C., Thapa,R.K., Nguyen,V., Yu,K., Yuan,Z.-C., Kohalmi,S.E., Liu,J., Marsolais,F. *et al.* (2019) RNA polymerase II-independent recruitment of SPT6L at transcription start sites in Arabidopsis. *Nucleic Acids Res.*, **47**, 6714–6725.